Geophysical Research Letters

RESEARCH LETTER
10.1029/2023GL104900

Secondary Brown Carbon Formation From Photooxidation of Furans From Biomass Burning

T. Joo[1,2], J. E. Machesky[3], L. Zeng[1,4], T. Hass-Mitchell[3], R. J. Weber[1], D. R. Gentner[3], and N. L. Ng[1,5,6]

[1]School of Earth and Atmospheric Sciences, Georgia Institute of Technology, Atlanta, GA, USA, [2]Now at Department of Chemical and Environmental Engineering, Yale University, New Haven, CT, USA, [3]Department of Chemical and Environmental Engineering, Yale University, New Haven, CT, USA, [4]Now at State Key Joint Laboratory of Environmental Simulation and Pollution Control, International Joint Research Center for Atmospheric Research (IJRC), College of Environmental Sciences and Engineering, Peking University, Beijing, China, [5]School of Chemical and Biomolecular Engineering, Georgia Institute of Technology, Atlanta, GA, USA, [6]School of Civil and Environmental Engineering, Georgia Institute of Technology, Atlanta, GA, USA

Abstract Furans are a major class of volatile organic compounds emitted from biomass burning. Their high reactivity with atmospheric oxidants leads to the formation of secondary organic aerosol (SOA), including secondary brown carbon (BrC) that can affect global climate via interactions with solar radiation. Here, we investigate the optical properties and chemical composition of SOA generated via photooxidation of furfural, 2-methylfuran, and 3-methylfuran under dry (RH < 5%) and humid (RH ~ 50%) conditions in the presence of nitrogen oxides (NO_x) and ammonium sulfate seed aerosol. Dry furfural oxidation has the greatest BrC formation, including reduced nitrogen-containing organic compounds (NOCs) in SOA, which are dominated by amines and amides formed from reactions between carbonyls and ammonia/ammonium. Based on the products detected, we propose novel formation pathways of NOCs in furfural photooxidation, which can contribute to BrC via accretion reactions during the photochemical aging of biomass burning plumes.

Plain Language Summary Biomass burning is a substantial source of both gas- and particle-phase carbon to the atmosphere, including light-absorbing aerosol known as brown carbon. Brown carbon can be emitted directly from combustion activities and also formed through the oxidation of gas-phase carbon, known as secondary brown carbon. In this study, we investigate secondary brown aerosol formation from furans (chemicals with a five-membered aromatic ring with four carbon atoms and one oxygen atom), one of the major classes of gaseous compounds emitted from biomass burning. We find that furfural is an important subset of furans that generates substantial brown carbon during oxidation, with corresponding formation of nitrogen-containing organic compounds.

Key Points:

- Photooxidation of furans in the presence of NO_x and ammonium sulfate aerosol leads to secondary brown carbon formation
- Optical properties of secondary brown carbon from furfural photooxidation are comparable to ambient biomass burning observations
- Reduced nitrogen species are associated with brown carbon formation from furfural photooxidation and are enhanced under dry conditions

Supporting Information:

Supporting Information may be found in the online version of this article.

Correspondence to:

N. L. Ng,
ng@chbe.gatech.edu

Citation:

Joo, T., Machesky, J. E., Zeng, L., Hass-Mitchell, T., Weber, R. J., Gentner, D. R., & Ng, N. L. (2024). Secondary brown carbon formation from photooxidation of furans from biomass burning. *Geophysical Research Letters*, *51*, e2023GL104900. https://doi.org/10.1029/2023GL104900

Received 12 JUN 2023
Accepted 18 NOV 2023

1. Introduction

Biomass burning is a major source of gas- and particle-phase carbon in the atmosphere (Akagi et al., 2011; Reddington et al., 2016). It impacts both climate and air quality and is expected to increase with climate change (Abatzoglou & Williams, 2016). Biomass burning is also the major source of brown carbon (BrC), which can contribute to positive climate forcings by absorbing solar radiation in near-ultraviolet (UV, 300–400 nm) to visible (400–700 nm) range (Feng et al., 2013; Laskin et al., 2015; Zeng et al., 2020). Atmospheric BrC sources include primary organic aerosol emission and secondary organic aerosol (SOA) formation. Humic-like substances (HULIS) formation via in-cloud processing is a well-known important source of secondary BrC, while nitrogen-containing aromatic compounds and particle-phase reactions of organics with carbonyl moieties in the presence of ammonium are also recognized to be significant sources of secondary BrC (De Haan et al., 2020; Galloway et al., 2009; Hoffer et al., 2006; Laskin et al., 2015; Palm et al., 2020; Updyke et al., 2012). As thousands of volatile organic compounds (VOCs) are emitted from biomass burning plumes (Hayden et al., 2022), the formation and aging process of BrC in the atmosphere is complicated, contributing to the large uncertainties in aerosol radiative impact in current climate models (Boucher et al., 2013).

Biomass burning SOA has been proposed to largely originate from the oxidation of understudied VOCs such as phenols or furans (Akherati et al., 2020; Bruns et al., 2016; Hatch et al., 2017). Furans are a major class of heterocyclic compounds in biomass burning emissions that are generated from pyrolysis of cellulose (Ciccioli

Table 1
Summary of Experimental Conditions

Precursor	Initial NO_x (ppb)	RH (%)	Injected hydrocarbon (HC) (ppb)[a]	ΔHC (ppb)	Organic mass concentration during filter collection (μg/m^3)[b]
Furfural	576	<5	294.8 ± 6.3	212.4 ± 6.3	78.9 ± 6.5
Furfural	540	53	246.0 ± 2.8	163.6 ± 2.8	194.1 ± 19.7
2-methylfuran	734	<5	537.0 ± 7.1	537.0 ± 7.1	34.5 ± 3.7
2-methylfuran	774	53	588.4 ± 5.9	588.4 ± 5.9	72.1 ± 9.2
3-methylfuran	964	<5	629.2 ± 9.5	629.2 ± 9.5	85.1 ± 15.0
3-methylfuran	741	46	621.6 ± 7.3	621.6 ± 7.3	86.2 ± 14.4

[a]HC uncertainties are calculated based on the calibration error and 1σ of HC concentrations prior to photooxidation. [b]The density of 2- and 3-methylfuran SOA (ρ_{SOA}) is adopted from a previous work (1.23 ± 0.09 and 1.34 ± 0.14 g/cm^3, respectively) (Gómez Alvarez et al., 2009), and that of furfural SOA (1.35 ± 0.1 g/cm^3) is estimated from additional dry and humid nucleation experiments using the method in Bahreini et al. (2005). 1 m^3 of chamber air volume is drawn through the filters in each experiment. The uncertainties shown for organic mass concentration are calculated from 1σ of aerosol volume measured by the SMPS during the filter collection and uncertainties in ρ_{SOA}.

et al., 2001; Gilman et al., 2015; Hatch et al., 2017; Mettler et al., 2012) and are prevalent in other environments (e.g., tobacco smoke and indoor air) (Sheu et al., 2021, 2022). This class of compounds is highly reactive with atmospheric oxidants and can produce high yields of carbonyls that can further react to form BrC in the presence of ammonium (Aschmann et al., 2014; De Haan et al., 2020; Decker et al., 2019; Gómez Alvarez et al., 2009; Jiang, Tsona, et al., 2019; Koss et al., 2018; Laskin et al., 2015; Lee et al., 2013; Updyke et al., 2012). Hence, furan oxidation has the potential to serve as an important source of secondary BrC, but the optical properties of furans SOA formed via photooxidation have not been investigated, with studies limited thus far to nighttime oxidation (Chen, Mayorga, et al., 2022; Chen, Raeofy, et al., 2022; Jiang, Frie, et al., 2019).

The overall aim of this work is to improve understanding of the chemical composition and optical properties of SOA derived from biomass burning plumes via daytime oxidation and aging. Specifically, we investigate secondary BrC formation from photooxidation of major furans emitted from biomass burning: furfural, 2-methylfuran, and 3-methylfuran (Ciccioli et al., 2001; Decker et al., 2019; Gilman et al., 2015). Laboratory chamber experiments are conducted to generate SOA under different humidity conditions with filter sampling and subsequent offline analysis to examine the light-absorbing properties of furans SOA. Aerosol chemical composition is measured using both online and offline techniques in order to identify species and molecular functionalities associated with BrC formation.

2. Materials and Methods

2.1. Environmental Chamber Experiments

Experiments are performed in the Georgia Tech Environmental Chamber (GTEC) facility (Boyd et al., 2015) at 22°C under dry (RH<5%) and humid (RH ~ 50%) conditions (Table 1). Ammonium sulfate ($(NH_4)_2SO_4$) seed aerosol is injected into the chamber by atomizing a 0.015 M solution without a dryer downstream of the atomizer. The particle number and volume concentrations following 20 min of atomization under dry conditions are typically ~20,000 cm^{-3} and ~20 μm^3/cm^3, respectively. Substantially higher seed particle volume concentrations (~35 μm^3/cm^3) are observed in humid experiments due to the deliquesced nature of $(NH_4)_2SO_4$ (Takeuchi & Ng, 2019). The desired amount of 2-furanaldehyde (furfural, 99%, Sigma-Aldrich), 2-methylfuran (99%, Sigma-Aldrich), and 3-methylfuran (98%, ACROS) is injected into a glass bulb and then carried into the chamber via pure air flow. HONO, which has been reported as the dominant contributor to the hydroxyl radical (OH) in wildfire plumes, especially in the early stage of oxidation (Palm et al., 2020; Peng et al., 2020), is injected as an OH precursor ([OH] = 6×10^6–10^7 molecules/cm^3 in the chamber). HONO is synthesized by dripping 1% wt $NaNO_2$ (VWR International) into 10% wt H_2SO_4 (VWR International) in a glass bulb at a volume ratio of 1:2. Pure air is then passed over the mixture solution to introduce HONO into the chamber (Tuet et al., 2017). During the HONO synthesis, NO and NO_2 are formed as byproducts, and initial NO_x/VOC of the experiments range from 1.2 to 2.2, similar to the range reported from combustion studies (Coggon et al., 2019; Tiitta et al., 2016). In each experiment, aerosol filter samples are collected onto two 47 mm Teflon filters (2 μm pore size, Pall Corporation) simultaneously using a flow splitter (1100, Brechtel) around the time of the maximum aerosol mass concentration. Filter samples are stored in a freezer (≤−15°C) until the analysis.

2.2. Instrumentation

One set of filters is cut into halves and each half is extracted with water or methanol to measure the light absorption spectra using a 2.5-m path-length liquid waveguide capillary cell (LWCC, World Precision). A deuterium tungsten halogen light source (DT-Mini, Ocean Optics) and a light detector (USB4000, Ocean Optics) are coupled with the LWCC to continuously monitor 230–800 nm wavelength. Light absorption coefficient (Abs_λ) of each solution is calculated following Hecobian et al. (2010) (detailed in Supporting Information S1). Absorption

Ångström exponents (AAE) are determined by fitting Abs_λ with a power law as shown in Figure S1 in Supporting Information S1. To account for the dependency of Abs_λ on the mass concentration (C_M), mass absorption efficiency (MAE = Abs_λ/C_M) is estimated. The imaginary refractive index (k_λ), which is the absorption component of the refractive index, is calculated using Equation 1 to facilitate a comparison of the light-absorbing properties of furans SOA in this study with previous studies. ρ_{SOA} is obtained from Gómez Alvarez et al. (2009) and additional nucleation experiments following the method in Bahreini et al. (2005) (Table 1).

$$k_\lambda = \frac{\rho_{SOA} \cdot \lambda \cdot Abs_\lambda}{4\pi \cdot C_M} = \frac{\rho_{SOA} \cdot \lambda}{4\pi} \cdot MAE \quad (1)$$

The other set of filters is extracted with methanol for offline chemical composition analysis by a liquid chromatography coupled with electrospray ionization and high-resolution quadrupole time-of-flight tandem mass spectrometry (LC-ESI-Q-ToF, Agilent 1260 Infinity LC and Agilent 6550 Q-ToF) (Ditto et al., 2018). Agilent Poroshell 120 SB-Aq reverse-phase column is used for LC, and the analysis is performed in both positive and negative ionization modes. The MS mode (ToF only) and MS/MS mode (tandem MS mode) are applied for the analysis of OA extracts to identify speciated composition and functional group distribution, respectively (Ditto et al., 2022). Ions detected in the MS mode that are validated through blank subtraction and quality assurance/quality control (QA/QC) processes are selected for MS/MS analysis (performed via auto MS/MS preferred-list-only mode from Agilent Masshunter acquisition mode) using the retention time and *m/z*. For this analysis, an average of 77% of compounds observed in MS mode are selected for MS/MS mode analysis based on the molecular feature score, structure score, and separation results of compounds (oxygen- or nitrogen-containing) having high signal abundance from MS mode. The MS/MS spectra are imported into SIRIUS with CSI: Finger-ID for molecular structure prediction, which can provide information on functional group distribution with high probability (Dührkop et al., 2015, 2019a; Hoffmann et al., 2022; Schymanski et al., 2017). Details of filter extractions, instrument conditions, data processing, and QA/QC have been discussed previously (Ditto et al., 2018, 2020, 2022).

Aerosol chemical composition is continuously measured using a High-Resolution Time-of-Flight Aerosol Mass Spectrometer (HR-ToF-AMS, Aerodyne Research Inc.) (Canagaratna et al., 2015; DeCarlo et al., 2006). A Filter Inlet for Gases and AEROsols (FIGAERO) (Lopez-Hilfiker et al., 2014) coupled with a High-Resolution Time-of-Flight iodide Chemical Ionization Mass Spectrometer (HR-ToF-CIMS, Aerodyne Research Inc.) is used to measure gas-phase and particle-phase oxidized organic composition. FIGAERO collects particles on a PTFE filter (Pall Corp., Zefluor 25 mm, 2 μm pore-size) while measuring gas-phase species from HR-ToF-CIMS, followed by a thermal desorption cycle to measure particle-phase species. Volatility distribution is estimated as saturation mass concentration (C*, $\mu g/m^3$) from the temperature corresponding to the signal peak (T_{max}) obtained during the desorption cycle of known compounds. The operation of FIGAERO-CIMS and the C* estimation calibration were detailed in previous studies (Joo et al., 2019; Stark et al., 2017; Takeuchi & Ng, 2019).

A scanning mobility particle sizer (SMPS) consisting of a differential mobility analyzer (DMA) (TSI 3040) and a condensation particle counter (CPC) (TSI 3775) is operated to monitor size-dependent particle number and volume concentrations. We note that a dryer is not attached at the inlet of all particle-sampling instruments to avoid loss of semi-volatile compounds and alteration in particle-phase aqueous reactions during the drying process (Faust et al., 2017; Zhang et al., 2011). The amount of precursor VOC is monitored using a gas chromatograph-flame ionization detector (GC-FID, Agilent 7890A) with a PLOT-Q column (Agilent). A cavity attenuated phase shift monitor (CAPS; Aerodyne Research Inc.) (Kebabian et al., 2005) and a $NO\text{-}NO_2\text{-}NO_x$ Analyzer (42C, Thermo Fisher Scientific) measure NO_2 and NO, respectively.

3. Results and Discussion

3.1. Optical Properties of Furans SOA

The 3 furans tested form varying amounts of BrC under dry and humid conditions. Figure 1 and Table S1 in Supporting Information S1 summarize the MAE, AAE, and *k* values of furfural, 2-methylfuran, and 3-methylfuran SOA (methanol extracts) with water extract results shown in Figure S2 in Supporting Information S1. Here, we focus on discussing methanol extracts results as they show stronger light-absorbing properties. Furfural SOA exhibits the highest MAE throughout the 300–700 nm wavelength range, followed by 2-methylfuran and 3-methylfuran SOA (Figure 1a). For each precursor, additionally, MAE is observed to be higher for SOA formed

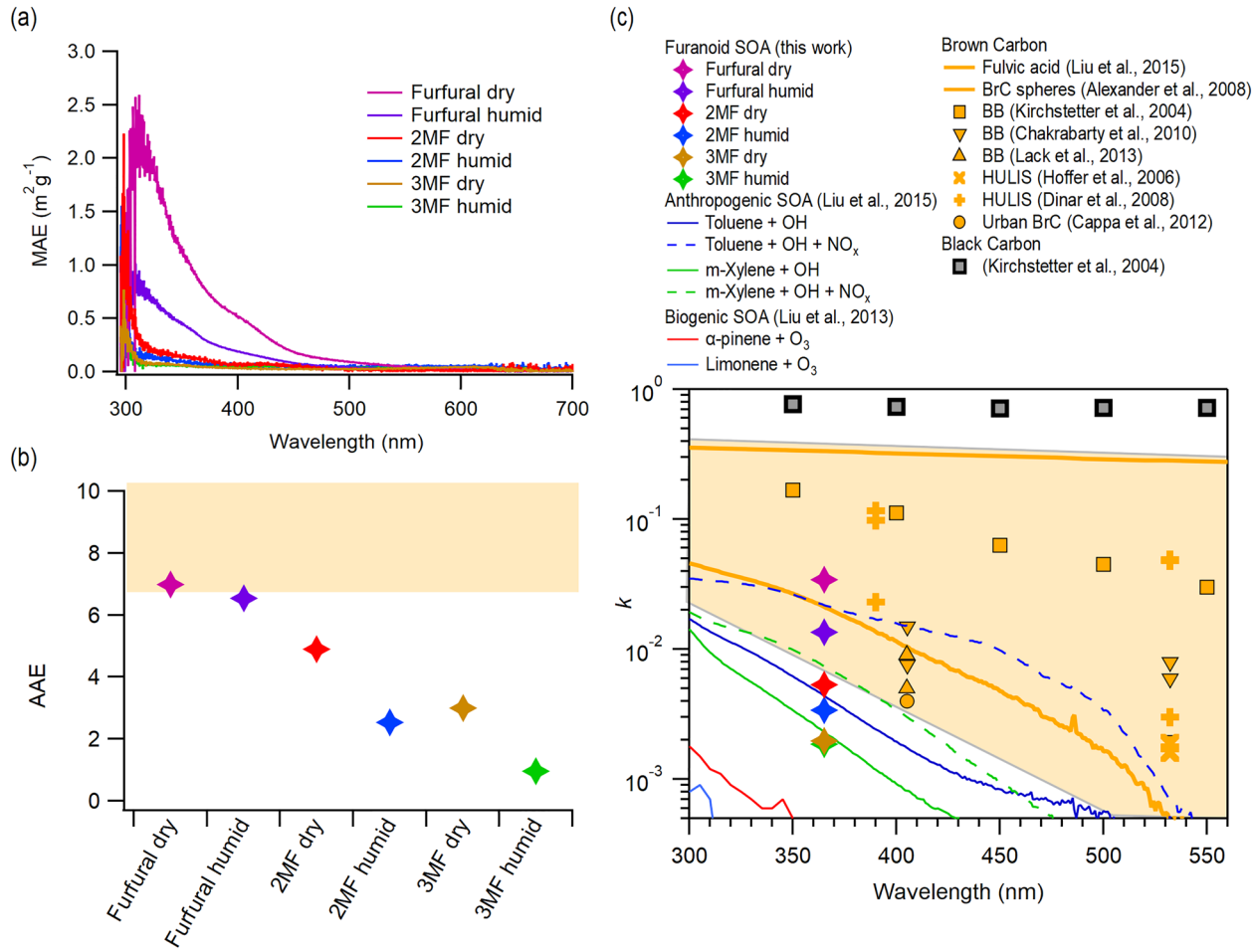

Figure 1. (a) Mass absorption efficiency (MAE), (b) absorption Ångström exponents (AAE) of furans SOA (methanol extracts), and (c) comparison of imaginary refractive index *k* of furans SOA with previous studies. "2MF" refers to 2-methylfuran and "3MF" refers to 3-methylfuran oxidation experiments. Dry and humid correspond to the chamber relative humidity under which the SOA is formed. Shaded regions in (b) and (c) represent the range of atmospheric BrC (Reprinted with permission from Liu et al. (2015) Copyright 2015 Copernicus Publications).

under dry conditions than humid conditions. The calculated AAE, which depends solely on the types of chromophores (Hecobian et al., 2010), follows similar trends as MAE (Figure 1b). It is noted that humid 2-methylfuran SOA and dry and humid 3-methylfuran SOA have substantially lower AAE than the other furans SOA. Among all the experiments, only furfural SOA exhibits AAE that approaches the regime of laboratory-generated smoke or biomass-burning HULIS (shaded region in Figure 1b, AAE = 7–16) (Chen & Bond, 2010; Hoffer et al., 2006).

We further estimate *k* in order to compare the light absorption of furans SOA with atmospherically relevant light-absorbing materials (Figure 1c). Here, we report k_{365} (average of *k* between 360 and 370 nm) as the representative absorption property of furans SOA. We chose this wavelength range since it is sufficiently far from the UV region, which avoids interferences from non-organic compounds, and is comparable to the range used in previous studies (Hecobian et al., 2010; Laskin et al., 2015; Liu et al., 2016, 2021). Overall, the k_{365} values of furans SOA are higher than those of biogenic SOA, but they are comparable to the *k* values of anthropogenic SOA. Specifically, k_{365} of furfural SOA is comparable to that of toluene/m-xylene SOA formed in the presence of NO_x whereas k_{365} of methylfurans SOA is comparable to toluene/m-xylene SOA formed without NO_x. Among the furans SOA, only the k_{365} values of furfural SOA are within the range of atmospheric BrC. Taken together with the higher furfural emissions from biomass burning (Ciccioli et al., 2001; Decker et al., 2019; Gilman et al., 2015) and similar or higher SOA formation at lower initial concentration compared to methylfurans (Table 1), our results highlight that the photooxidation of furfural can be an important source of secondary BrC during photochemical processing of biomass burning plumes, especially when the biomass burning event and following oxidation occur under lower humidity conditions (e.g., California Williams Fire (Akagi et al., 2012)).

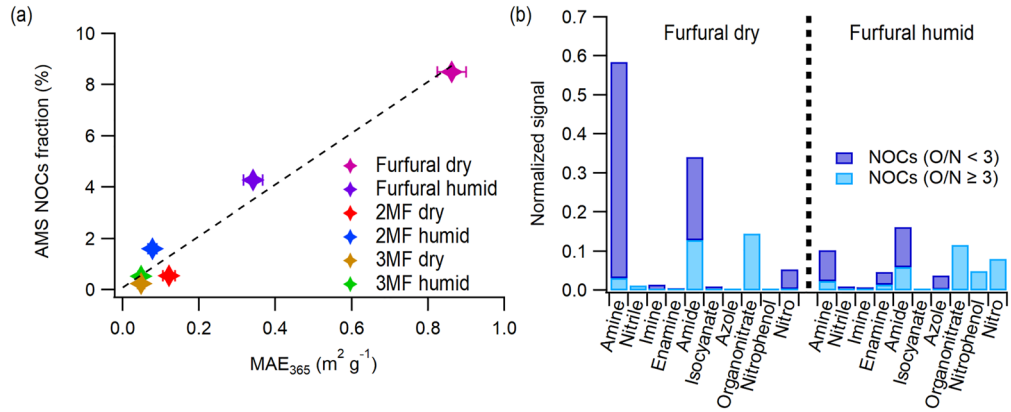

Figure 2. (a) Relationship between the fraction of nitrogen-containing organic compounds (NOCs) observed as NOCs-related ions via AMS versus MAE_{365}. (b) Nitrogen-containing functional group distribution of furfural SOA under dry (left) and humid (right) conditions. Ion abundance of compounds with each functional group type is normalized by the total ion abundance measured via LC-ESI-Q-ToF (MS mode).

3.2. Relationship Between Bulk SOA Chemical Composition and Optical Properties

Bulk furans SOA composition measurements using HR-ToF-AMS reveal a correspondence between light-absorbing properties and nitrogen-containing organic compounds (NOCs). Specifically, we observe a linear relationship between MAE at 365 nm (MAE_{365}) and the fraction of NOCs-related ions (i.e., $C_xH_yN_n^+$ and $C_xH_yO_zN_n^+$ ion types) in furans SOA (Figure 2a). NOCs-related ions could arise from amines, amides, amino acids, or nitro functionalities fragmentation during the electron ionization impaction (70 eV) of vaporized particles in HR-ToF-AMS (Xu et al., 2021). As only a small portion of nitro functionalities can be measured as NO^+ and NO_2^+ ions (Xu et al., 2021), these ions are excluded when estimating NOCs fraction as they dominantly correspond to organonitrate (Farmer et al., 2010), which are reported to be small contributors to light-absorbing properties (Liu et al., 2012, 2021). Furfural SOA shows the highest fraction of NOCs-related ions (8% and 4% for dry and humid conditions, respectively) and MAE_{365} (0.86 m^2/g and 0.34 m^2/g for dry and humid conditions, respectively). Whereas, the NOCs fraction and MAE_{365} of 2- and 3-methylfuran SOA are less than 2% and 0.2 m^2/g, respectively. While the fraction of NOC-related ions in furans SOA is lower than other prominent ion types (i.e., $C_xH_y^+$, $C_xH_yO_z^+$) (Figure S3 in Supporting Information S1), previous studies reported that NOCs-related functional groups can be the main components of BrC chromophores despite the small mass fractions of NOCs-related ions (i.e., fragments) in aerosol (Laskin et al., 2015; Liu et al., 2021; Palm et al., 2020).

NOCs-related ions are predominated by $C_xH_yN_n^+$ ion type, contributing 6% and 3% to furfural SOA formed under dry and humid conditions, respectively (Figure S3 in Supporting Information S1). Such contributions are largely comprised of *m/z* 27 (CHN^+) and two clusters around *m/z* 40 ($C_2H_2N^+$) and 52 ($C_3H_2N^+$). Meanwhile, the $C_xH_yN_n^+$ ion type contributes ≤1% in 2-methylfuran and 3-methylfuran SOA without apparent clusters. The $C_xH_yN_n^+$ ion type has been reported as an important contributor to BrC in glyoxal-$(NH_4)_2SO_4$ droplets and SOA formed from photochemical oxidation of toluene (Lee et al., 2013; Liu et al., 2021). This ion type can correspond to compounds with C-N bonds that enhance light absorption (Galloway et al., 2009; Laskin et al., 2015; Nozière et al., 2009). Specifically, glyoxal-$(NH_4)_2SO_4$ droplet experiments showed large contributions of *m/z* 27 (CHN^+), 41 ($C_2H_3N^+$), and 68 ($C_3H_4N_2^+$), while toluene SOA had large contributions of *m/z* 27 (CHN^+), 41 ($C_2H_3N^+$), and 43 ($C_2H_5N^+$) (Lee et al., 2013; Liu et al., 2021). Despite the difference in $C_xH_yN_n^+$ ion type distribution, glyoxal SOA and furfural SOA share a similar humidity dependency of light-absorbing properties, showing a stronger absorbance when the SOA is formed under dry conditions (De Haan et al., 2020), whereas toluene SOA shows a higher MAE_{365} when formed under humid conditions (Liu et al., 2016). The similarity in light absorption spectra response between furfural SOA and glyoxal SOA under humid conditions may indicate that these two precursors produce SOA with more similar optical and chemical characteristics compared to toluene SOA.

We further perform offline analysis of SOA filter samples using LC-ESI-Q-ToF, focusing on furfural SOA since it exhibits both AAE and *k* values that approach the ranges reported for ambient biomass burning samples (Figure 1). The MS-mode results identify a wide range of molecular sizes (C_4–C_{30}), which is dominated by CHON compounds

(Figure S4 in Supporting Information S1). These CHON compounds are further categorized into less-oxygenated versus more-oxygenated subgroups, using the O/N ratio of organonitrate to delineate the two, though O/N ≥ 3 compounds may contain a reduced nitrogen atom and multiple other oxygen-containing groups rather than an organonitrate functional group (Ditto et al., 2022). Overall, O/N < 3 compounds dominate dry furfural SOA (45.7%) and O/N ≥ 3 compounds dominate humid furfural SOA (46.9%) (Figure S4 in Supporting Information S1). MS/MS-mode results exhibit the distribution of nitrogen-containing functional groups for furfural SOA formed under dry and humid conditions (Figure 2b). Generally, dry furfural SOA has substantial contributions from reduced nitrogen-containing functional groups (i.e., amines, amides) containing C-N bonds, followed by organonitrate and nitro functional groups. Among these functional groups, the abundance of amines and amides suggests humidity dependence, being substantially enhanced in dry conditions. We also observe more compounds containing imines, another reduced nitrogen functionality with C-N bonds, among the total number of identified compounds in dry furfural SOA (Figure S5 in Supporting Information S1). For NOCs in humid furfural SOA, we also observe the presence of enamine, azole, and nitrophenol groups in addition to amine, amide, organonitrate, and nitro functional groups.

It is noted that reduced NOCs in furfural SOA would have been most often measured as $C_xH_yN_n^+$ ion type in HR-ToF-AMS owing to hard ionization that induces a significant level of fragmentation of the parent compounds compared to electrospray ionization used for LC-ESI-Q-ToF. Nevertheless, results of bulk composition analysis from both HR-ToF-AMS and LC-ESI-Q-ToF demonstrate that reduced nitrogen-containing compounds possessing C-N bonds can be substantial among NOCs in furfural SOA and correspond to BrC. The greater abundance of amines and amides and higher MAE_{365} for dry furfural SOA suggest that the presence of these functional groups potentially governs the light-absorbing properties of furfural SOA. Furthermore, the presence of aerosol liquid water under humid conditions could have facilitated additional reactions to generate a variety of nitrogen-containing functional groups.

3.3. Particle-Phase Pathways Yielding Reduced C_5 NOCs in Furfural SOA

A simplified NOCs formation mechanism during furfural photooxidation is proposed in Figure 3a. The carbonyl functionality in furfural and 4-oxo-2-pentendial, which is a first-generation oxidation product from furfural photooxidation detected by the HR-ToF-CIMS in the gas phase and also reported by Zhao and Wang (2017), can interact with NH_3 (present as NH_3 (aq) or NH_4^+ in seed aerosol) (Lee et al., 2013) and generate amines in a hemiaminal form ($C_5H_7NO_2$ and $C_5H_7NO_3$). $C_5H_7NO_2$ and $C_5H_7NO_3$ can then undergo accretion reactions or dehydration to form imines (C_5H_5NO and $C_5H_5NO_2$) that can be followed by N-heterocyclic compounds formation and further accretion reactions (Bones et al., 2010; Kampf et al., 2016; Laskin et al., 2015; Lee et al., 2013; Updyke et al., 2012). The NOCs in Figure 3a possess C-N bonds that can enhance light absorption (Galloway et al., 2009; Laskin et al., 2015; Nozière et al., 2009) and can participate in reactions to form high-molecular-weight compounds observed by LC-ESI-Q-ToF (Figure S4 in Supporting Information S1), similar to the reactions reported during α-dicarbonyls (glyoxal, methylglyoxal, etc.) photooxidation in the presence of NH_3/NH_4^+ (De Haan et al., 2020; Laskin et al., 2015; Lee et al., 2013; Updyke et al., 2012).

Among the NOCs in Figure 3a, we find that a small portion of amines can exist as monomers in the particle phase (Figure S6 in Supporting Information S1). Nevertheless, thermograms (Figure 3b) show that they are mostly associated with high-molecular-weight NOCs as the C* of amines are skewed toward the extremely low-VOC (ELVOC) region (Donahue et al., 2012) with multi-peak-pattern thermograms (Figure S6b–S6e in Supporting Information S1) and having higher T_{max} ($C_5H_7NO_2$: 128.4°C, $C_5H_7NO_3$: 82.7°C) than that of C_5 calibrant (glutaric acid, $C_5H_8O_4$, 43°C) obtained during FIGAERO calibration. We also identify formulas that correspond to imines (C_5H_5NO and $C_5H_5NO_2$), but they likely arise from fragmentation of accretion products, showing negligible signals at high-C* (low T_{max}) region (Figure 3b). Measurement of the proposed amines and imines can result from the fragmentation of amides or enamines observed in Figure 2b, which are formed by the reaction of amines with carboxylic acids or carbonyls, respectively (Barsanti & Pankow, 2006; Bones et al., 2010; Price et al., 2014). Furthermore, Mannich-type reaction and aldol condensation, which are reported to enhance light absorption at 300–400 nm (Nozière & Esteve, 2007; Nozière et al., 2010), are other forms of accretion reactions that the proposed C_5 amines and imines can participate in.

The browning reactions described here, including amine/imine formation and their accretion reactions, are typically considered aqueous processes (Laskin et al., 2015). Accordingly, amines ($C_5H_7NO_2$ and $C_5H_7NO_3$) in the particle phase are more rapidly formed under humid conditions than under dry conditions, where amine-related compounds reach their maximum signal immediately when oxidation begins in humid conditions (Figure 3c). However, De Haan et al. (2020) found that Maillard chemistry can also occur on the surface of dry $(NH_4)_2SO_4$

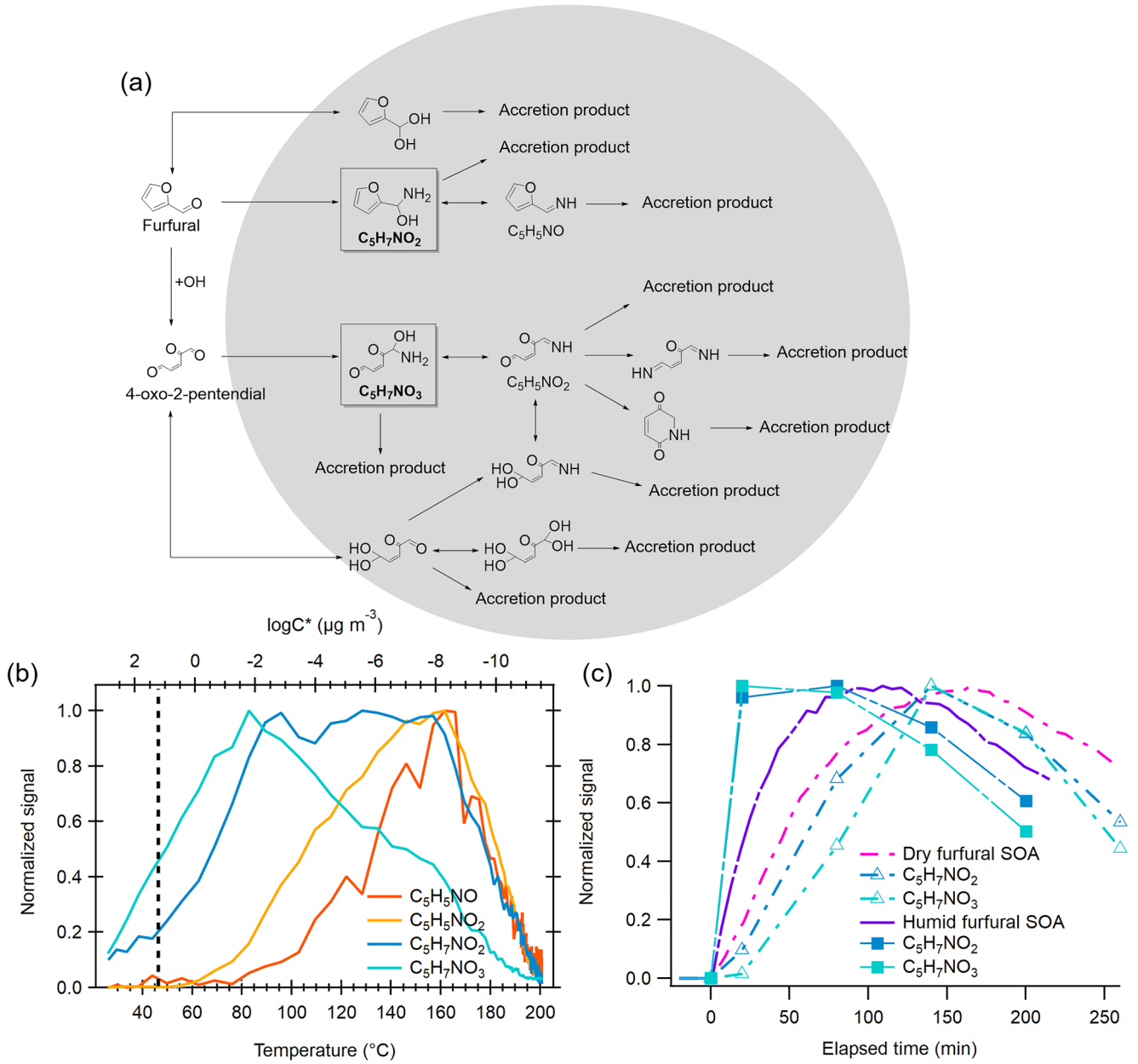

Figure 3. (a) Proposed uptake and reaction pathway of furfural and 4-oxo-2-pentendial to $(NH_4)_2SO_4$ seed aerosol. Boxed compounds are detected by FIGAERO-CIMS. (b) Thermogram of C_5H_5NO, $C_5H_5NO_2$, $C_5H_7NO_2$, $C_5H_7NO_3$ in dry furfural SOA. Dashed line refers to the T_{max} of C_5 calibrant (glutaric acid, $C_5H_8O_4$). (c) Time series of particle-phase compounds (from FIGAERO-CIMS) with SOA mass concentration (calculated from SMPS volume concentration and ρ_{SOA}).

seed aerosol, where glyoxal can access and deplete a trace amount of water. Similarly, furfural and its oxidation products may undergo such processes to enhance aerosol browning under dry conditions. We additionally note that 2-methylfuran and 3-methylfuran can participate in similar reactions in the particle phase owing to the formation of dicarbonyls during photooxidation (Aschmann et al., 2014; Gómez Alvarez et al., 2009), although the difference in the reactivity of carbonyls in particle phase may have led to their reduced optical properties compared to furfural SOA (Hensley et al., 2021).

4. Conclusions

To our knowledge, this is the first study to demonstrate secondary BrC formation from photochemical oxidation of furans. Among the major furans (furfural, 2-methylfuran, and 3-methylfuran) emitted from biomass burning,

we find that furfural generates the most SOA and BrC chromophores. Combined with the higher emission rate of furfural compared to 2- and 3-methylfuran from biomass burning (Gilman et al., 2015; Hatch et al., 2017), the results in this study suggest that furfural can potentially serve as one of the most important SOA precursors among furans emitted from biomass burning. The stronger light absorption of furfural SOA corresponds to a higher fraction of reduced NOCs, dominated by amines and amides. Formation of such reduced NOCs likely contributes to the MAE values of furfural SOA formed via photooxidation, being 4–10 times higher than that formed via nighttime oxidation, where conjugated carbonyls were reported to be the main BrC chromophores (Chen, Mayorga, et al., 2022; Chen, Raeofy, et al., 2022). The nitrogen-containing functional group formation is driven by reactions between NH_3/NH_4^+ from $(NH_4)_2SO_4$ seed aerosol and the carbonyl functionality in furfural and its oxidation products. While there are considerable variations between plumes based on fire type, intensity, and location, a possible region where the reactions studied could occur is where the smoke plumes age and mix with background air, and contributions from the smoke plumes and background air are in more similar portions. For example, Xu et al. (2022) showed that OH exposure can be high at the edge of plumes and Pratt et al. (2011) reported the fraction of inorganic components in aerosol increased from 5.9% to 27.4% as the plume aged, which can be the results of both mixing with background air during plume dilution and secondary processes (Akagi et al., 2012; Falkovich et al., 2005; Fiedler et al., 2011; Souri et al., 2017). In these regions, species from smoke plumes, such as furans and NO_x, can still be enhanced and react in the presence of pre-existing $(NH_4)_2SO_4$ to form reduced NOCs. This oxidation process can continue over large spatial scales as the plumes continue to mix with the background air, and VOCs still remain and can continue to be oxidized in the presence of background inorganic aerosol. Functionalities in furfural NOCs further trigger reactions to form accretion products such as amides and enamines that have lower volatility, resulting in increased SOA mass concentration along with BrC formation. Accordingly, furfural photooxidation products can interact with other functionalized compounds and enhance the amount of SOA and BrC in biomass burning plumes, eventually extending the lifetime of biomass burning BrC via the generation of high-molecular-weight compounds (Di Lorenzo & Young, 2016; Wong et al., 2019). Future studies warrant more attention to the formation of reduced NOCs in the presence of various pre-existing aerosol given their diverse, yet variable, existence (e.g., Ditto et al. (2020); Ditto et al. (2022); Lee et al. (2013)) and continuous measurements of the light absorption during oxidation of furans, or other photochemically driven processes, as BrC chromophores can be both bleached and enhanced during these processes (Hems et al., 2021; Laskin et al., 2015; Updyke et al., 2012; Wong et al., 2019), which could strongly influence the overall optical importance of these compounds throughout their atmospheric lifespan.

Data Availability Statement

The chamber experiment data reported in this study are available at Joo et al. (2023) in the Index of Chamber Atmospheric Research in the United States (ICARUS) database (Nguyen et al., 2023). SIRIUS is used in this study for the LC-MS/MS data analysis (Dührkop et al., 2019b).

Acknowledgments
This research was funded by NSF AGS-1830727. The FIGAERO-HR-ToF-CIMS was purchased through NSF Major Research Instrumentation (MRI) Grant 1428738. D.R.G., J.E.M., and T. H-M. would like to acknowledge NSF AGS-1764126. L.Z. would like to acknowledge the financial support from the National Key Research and Development Program of China (2022YFC3701000, task4). The authors would like to thank Yuchen Wang for assistance in filter sample extraction, Masayuki Takeuchi for helpful discussion on the operation of FIGAERO-HR-ToF-CIMS and its data analysis, and Pengfei Liu for providing the literature data in Figure 1.

References

Abatzoglou, J. T., & Williams, A. P. (2016). Impact of anthropogenic climate change on wildfire across western US forests. *Proceedings of the National Academy of Sciences of the United States of America*, *113*(42), 11770–11775. https://doi.org/10.1073/pnas.1607171113

Akagi, S. K., Craven, J. S., Taylor, J. W., McMeeking, G. R., Yokelson, R. J., Burling, I. R., et al. (2012). Evolution of trace gases and particles emitted by a chaparral fire in California. *Atmospheric Chemistry and Physics*, *12*(3), 1397–1421. https://doi.org/10.5194/acp-12-1397-2012

Akagi, S. K., Yokelson, R. J., Wiedinmyer, C., Alvarado, M. J., Reid, J. S., Karl, T., et al. (2011). Emission factors for open and domestic biomass burning for use in atmospheric models. *Atmospheric Chemistry and Physics*, *11*(9), 4039–4072. https://doi.org/10.5194/acp-11-4039-2011

Akherati, A., He, Y., Coggon, M. M., Koss, A. R., Hodshire, A. L., Sekimoto, K., et al. (2020). Oxygenated aromatic compounds are important precursors of secondary organic aerosol in biomass-burning emissions. *Environmental Science and Technology*, *54*(14), 8568–8579. https://doi.org/10.1021/acs.est.0c01345

Alexander, D. T. L., Crozier, P. A., & Anderson, J. R. (2008). Brown carbon spheres in East Asian outflow and their optical properties. *Science*, *321*(5890), 833–836. https://doi.org/10.1126/science.1155296

Aschmann, S. M., Nishino, N., Arey, J., & Atkinson, R. (2014). Products of the OH radical-initiated reactions of furan, 2- and 3-methylfuran, and 2,3- and 2,5-dimethylfuran in the presence of NO. *The Journal of Physical Chemistry A*, *118*(2), 457–466. https://doi.org/10.1021/jp410345k

Bahreini, R., Keywood, M. D., Ng, N. L., Varutbangkul, V., Gao, S., Flagan, R. C., et al. (2005). Measurements of secondary organic aerosol from oxidation of cycloalkenes, terpenes, and m-xylene using an Aerodyne aerosol mass spectrometer. *Environmental Science and Technology*, *39*(15), 5674–5688. https://doi.org/10.1021/es048061a

Barsanti, K. C., & Pankow, J. F. (2006). Thermodynamics of the formation of atmospheric organic particulate matter by accretion reactions—Part 3: Carboxylic and dicarboxylic acids. *Atmospheric Environment*, *40*(34), 6676–6686. https://doi.org/10.1016/j.atmosenv.2006.03.013

Bones, D. L., Henricksen, D. K., Mang, S. A., Gonsior, M., Bateman, A. P., Nguyen, T. B., et al. (2010). Appearance of strong absorbers and fluorophores in limonene-O3 secondary organic aerosol due to NH4+-mediated chemical aging over long time scales. *Journal of Geophysical Research*, *115*(D5). https://doi.org/10.1029/2009JD012864

Boucher, O., Randall, D., Artaxo, P., Bretherton, C., Feingold, G., Forster, P., et al. (2013). Clouds and aerosols. In T. F. Stocker, D. Qin, G.-K. Plattner, M. Tignor, S. K. Allen, J. Boschung, et al. (Eds.), *Climate Change 2013: The Physical Science Basis. Contribution of Working Group I to the Fifth Assessment Report of the Intergovernmental Panel on Climate Change* (pp. 571–658). Cambridge University Press.

Boyd, C. M., Sanchez, J., Xu, L., Eugene, A. J., Nah, T., Tuet, W. Y., et al. (2015). Secondary organic aerosol formation from the β-pinene+NO_3 system: Effect of humidity and peroxy radical fate. *Atmospheric Chemistry and Physics*, *15*(13), 7497–7522. https://doi.org/10.5194/acp-15-7497-2015

Bruns, E. A., El Haddad, I., Slowik, J. G., Kilic, D., Klein, F., Baltensperger, U., & Prévôt, A. S. H. (2016). Identification of significant precursor gases of secondary organic aerosols from residential wood combustion. *Scientific Reports*, *6*(1), 27881. https://doi.org/10.1038/srep27881

Canagaratna, M. R., Jimenez, J. L., Kroll, J. H., Chen, Q., Kessler, S. H., Massoli, P., et al. (2015). Elemental ratio measurements of organic compounds using aerosol mass spectrometry: Characterization, improved calibration, and implications. *Atmospheric Chemistry and Physics*, *15*(1), 253–272. https://doi.org/10.5194/acp-15-253-2015

Cappa, C. D., Onasch, T. B., Massoli, P., Worsnop, D. R., Bates, T. S., Cross, E. S., et al. (2012). Radiative absorption enhancements due to the mixing state of atmospheric black carbon. *Science*, *337*(6098), 1078–1081. https://doi.org/10.1126/science.1223447

Chakrabarty, R. K., Moosmüller, H., Chen, L.-W. A., Lewis, K., Arnott, W. P., Mazzoleni, C., et al. (2010). Brown carbon in tar balls from smoldering biomass combustion. *Atmospheric Chemistry and Physics*, *10*(13), 6363–6370. https://doi.org/10.5194/acp-10-6363-2010

Chen, K., Mayorga, R., Raeofy, N., Lum, M., Woods, M., Bahreini, R., et al. (2022). Effects of nitrate radical levels and pre-existing particles on secondary Brown Carbon Formation from nighttime oxidation of furan. *ACS Earth and Space Chemistry*, *6*(11), 2709–2721. https://doi.org/10.1021/acsearthspacechem.2c00244

Chen, K., Raeofy, N., Lum, M., Mayorga, R., Woods, M., Bahreini, R., et al. (2022). Solvent effects on chemical composition and optical properties of extracted secondary brown carbon constituents. *Aerosol Science and Technology*, *56*(10), 917–930. https://doi.org/10.1080/02786826.2022.2100734

Chen, Y., & Bond, T. C. (2010). Light absorption by organic carbon from wood combustion. *Atmospheric Chemistry and Physics*, *10*(4), 1773–1787. https://doi.org/10.5194/acp-10-1773-2010

Ciccioli, P., Brancaleoni, E., Frattoni, M., Cecinato, A., & Pinciarelli, L. (2001). Determination of volatile organic compounds (VOC) emitted from biomass burning of mediterranean vegetation species by GC-MS. *Analytical Letters*, *34*(6), 937–955. https://doi.org/10.1081/AL-100103604

Coggon, M. M., Lim, C. Y., Koss, A. R., Sekimoto, K., Yuan, B., Gilman, J. B., et al. (2019). OH chemistry of non-methane organic gases (NMOGs) emitted from laboratory and ambient biomass burning smoke: Evaluating the influence of furans and oxygenated aromatics on ozone and secondary NMOG formation. *Atmospheric Chemistry and Physics*, *19*(23), 14875–14899. https://doi.org/10.5194/acp-19-14875-2019

DeCarlo, P. F., Kimmel, J. R., Trimborn, A., Northway, M. J., Jayne, J. T., Aiken, A. C., et al. (2006). Field-deployable, high-resolution, time-of-flight aerosol mass spectrometer. *Analytical Chemistry*, *78*(24), 8281–8289. https://doi.org/10.1021/ac061249n

Decker, Z. C. J., Zarzana, K. J., Coggon, M., Min, K.-E., Pollack, I., Ryerson, T. B., et al. (2019). Nighttime chemical transformation in biomass burning plumes: A box model analysis initialized with aircraft observations. *Environmental Science and Technology*, *53*(5), 2529–2538. https://doi.org/10.1021/acs.est.8b05359

De Haan, D. O., Hawkins, L. N., Jansen, K., Welsh, H. G., Pednekar, R., de Loera, A., et al. (2020). Glyoxal's impact on dry ammonium salts: Fast and reversible surface aerosol browning. *Atmospheric Chemistry and Physics*, *20*(16), 9581–9590. https://doi.org/10.5194/acp-20-9581-2020

Di Lorenzo, R. A., & Young, C. J. (2016). Size separation method for absorption characterization in brown carbon: Application to an aged biomass burning sample. *Geophysical Research Letters*, *43*(1), 458–465. https://doi.org/10.1002/2015GL066954

Dinar, E., Abo Riziq, A., Spindler, C., Erlick, C., Kiss, G., & Rudich, Y. (2008). The complex refractive index of atmospheric and model humic-like substances (HULIS) retrieved by a cavity ring down aerosol spectrometer (CRD-AS). *Faraday Discuss*, *137*, 279–295. https://doi.org/10.1039/b703111d

Ditto, J. C., Barnes, E. B., Khare, P., Takeuchi, M., Joo, T., Bui, A. A. T., et al. (2018). An omnipresent diversity and variability in the chemical composition of atmospheric functionalized organic aerosol. *Communications Chemistry*, *1*(1), 75. https://doi.org/10.1038/s42004-018-0074-3

Ditto, J. C., Joo, T., Slade, J. H., Shepson, P. B., Ng, N. L., & Gentner, D. R. (2020). Nontargeted tandem mass spectrometry analysis reveals diversity and variability in aerosol functional groups across multiple sites, seasons, and times of day. *Environmental Science and Technology Letters*, *7*(2), 60–69. https://doi.org/10.1021/acs.estlett.9b00702

Ditto, J. C., Machesky, J., & Gentner, D. R. (2022). Analysis of reduced and oxidized nitrogen-containing organic compounds at a coastal site in summer and winter. *Atmospheric Chemistry and Physics*, *22*(5), 3045–3065. https://doi.org/10.5194/acp-22-3045-2022

Donahue, N. M., Kroll, J. H., Pandis, S. N., & Robinson, A. L. (2012). A two-dimensional volatility basis set – Part 2: Diagnostics of organic-aerosol evolution. *Atmospheric Chemistry and Physics*, *12*(2), 615–634. https://doi.org/10.5194/acp-12-615-2012

Dührkop, K., Fleischauer, M., Ludwig, M., Aksenov, A. A., Melnik, A. V., Meusel, M., et al. (2019a). SIRIUS 4: A rapid tool for turning tandem mass spectra into metabolite structure information. *Nature Methods*, *16*(4), 299–302. https://doi.org/10.1038/s41592-019-0344-8

Dührkop, K., Fleischauer, M., Ludwig, M., Aksenov, A. A., Melnik, A. V., Meusel, M., et al. (2019b). SIRIUS 4 [Software]. github. https://github.com/boecker-lab/sirius/

Dührkop, K., Shen, H., Meusel, M., Rousu, J., & Böcker, S. (2015). Searching molecular structure databases with tandem mass spectra using CSI:FingerID. *Proceedings of the National Academy of Sciences of the United States of America*, *112*(41), 12580–12585. https://doi.org/10.1073/pnas.1509788112

Falkovich, A. H., Graber, E. R., Schkolnik, G., Rudich, Y., Maenhaut, W., & Artaxo, P. (2005). Low molecular weight organic acids in aerosol particles from Rondônia, Brazil, during the biomass-burning, transition and wet periods. *Atmospheric Chemistry and Physics*, *5*(3), 781–797. https://doi.org/10.5194/acp-5-781-2005

Farmer, D. K., Matsunaga, A., Docherty, K. S., Surratt, J. D., Seinfeld, J. H., Ziemann, P. J., & Jimenez, J. L. (2010). Response of an aerosol mass spectrometer to organonitrates and organosulfates and implications for atmospheric chemistry. *Proceedings of the National Academy of Sciences of the United States of America*, *107*(15), 6670–6675. https://doi.org/10.1073/pnas.0912340107

Faust, J. A., Wong, J. P. S., Lee, A. K. Y., & Abbatt, J. P. D. (2017). Role of aerosol liquid water in secondary organic aerosol Formation from volatile organic compounds. *Environmental Science and Technology*, *51*(3), 1405–1413. https://doi.org/10.1021/acs.est.6b04700

Feng, Y., Ramanathan, V., & Kotamarthi, V. R. (2013). Brown carbon: A significant atmospheric absorber of solar radiation? *Atmospheric Chemistry and Physics*, *13*(17), 8607–8621. https://doi.org/10.5194/acp-13-8607-2013

Fiedler, V., Arnold, F., Ludmann, S., Minikin, A., Hamburger, T., Pirjola, L., et al. (2011). African biomass burning plumes over the atlantic: Aircraft based measurements and implications for H_2SO_4 and HNO_3 mediated smoke particle activation. *Atmospheric Chemistry and Physics*, *11*(7), 3211–3225. https://doi.org/10.5194/acp-11-3211-2011

Galloway, M. M., Chhabra, P. S., Chan, A. W. H., Surratt, J. D., Flagan, R. C., Seinfeld, J. H., & Keutsch, F. N. (2009). Glyoxal uptake on ammonium sulphate seed aerosol: Reaction products and reversibility of uptake under dark and irradiated conditions. *Atmospheric Chemistry and Physics*, *9*(10), 3331–3345. https://doi.org/10.5194/acp-9-3331-2009

Gilman, J. B., Lerner, B. M., Kuster, W. C., Goldan, P. D., Warneke, C., Veres, P. R., et al. (2015). Biomass burning emissions and potential air quality impacts of volatile organic compounds and other trace gases from fuels common in the US. *Atmospheric Chemistry and Physics*, *15*(24), 13915–13938. https://doi.org/10.5194/acp-15-13915-2015

Gómez Alvarez, E., Borrás, E., Viidanoja, J., & Hjorth, J. (2009). Unsaturated dicarbonyl products from the OH-initiated photo-oxidation of furan, 2-methylfuran and 3-methylfuran. *Atmospheric Environment*, *43*(9), 1603–1612. https://doi.org/10.1016/j.atmosenv.2008.12.019

Hatch, L. E., Yokelson, R. J., Stockwell, C. E., Veres, P. R., Simpson, I. J., Blake, D. R., et al. (2017). Multi-instrument comparison and compilation of non-methane organic gas emissions from biomass burning and implications for smoke-derived secondary organic aerosol precursors. *Atmospheric Chemistry and Physics*, *17*(2), 1471–1489. https://doi.org/10.5194/acp-17-1471-2017

Hayden, K. L., Li, S. M., Liggio, J., Wheeler, M. J., Wentzell, J. J. B., Leithead, A., et al. (2022). Reconciling the total carbon budget for boreal forest wildfire emissions using airborne observations. *Atmospheric Chemistry and Physics*, *22*(18), 12493–12523. https://doi.org/10.5194/acp-22-12493-2022

Hecobian, A., Zhang, X., Zheng, M., Frank, N., Edgerton, E. S., & Weber, R. J. (2010). Water-Soluble Organic Aerosol material and the light-absorption characteristics of aqueous extracts measured over the Southeastern United States. *Atmospheric Chemistry and Physics*, *10*(13), 5965–5977. https://doi.org/10.5194/acp-10-5965-2010

Hems, R. F., Schnitzler, E. G., Liu-Kang, C., Cappa, C. D., & Abbatt, J. P. D. (2021). Aging of atmospheric Brown carbon aerosol. *ACS Earth and Space Chemistry*, *5*(4), 722–748. https://doi.org/10.1021/acsearthspacechem.0c00346

Hensley, J. C., Birdsall, A. W., Valtierra, G., Cox, J. L., & Keutsch, F. N. (2021). Revisiting the reaction of dicarbonyls in aerosol proxy solutions containing ammonia: The case of butenedial. *Atmospheric Chemistry and Physics*, *21*(11), 8809–8821. https://doi.org/10.5194/acp-21-8809-2021

Hoffer, A., Gelencsér, A., Guyon, P., Kiss, G., Schmid, O., Frank, G. P., et al. (2006). Optical properties of humic-like substances (HULIS) in biomass-burning aerosols. *Atmospheric Chemistry and Physics*, *6*(11), 3563–3570. https://doi.org/10.5194/acp-6-3563-2006

Hoffmann, M. A., Nothias, L.-F., Ludwig, M., Fleischauer, M., Gentry, E. C., Witting, M., et al. (2022). High-confidence structural annotation of metabolites absent from spectral libraries. *Nature Biotechnology*, *40*(3), 411–421. https://doi.org/10.1038/s41587-021-01045-9

Jiang, H., Frie, A. L., Lavi, A., Chen, J. Y., Zhang, H., Bahreini, R., & Lin, Y.-H. (2019). Brown Carbon Formation from nighttime chemistry of unsaturated heterocyclic volatile organic compounds. *Environmental Science and Technology Letters*, *6*(3), 184–190. https://doi.org/10.1021/acs.estlett.9b00017

Jiang, X., Tsona, N. T., Jia, L., Liu, S., Zhang, H., Xu, Y., & Du, L. (2019). Secondary organic aerosol formation from photooxidation of furan: Effects of NOx and humidity. *Atmospheric Chemistry and Physics*, *19*(21), 13591–13609. https://doi.org/10.5194/acp-19-13591-2019

Joo, T., Machesky, J. E., Zeng, L., Hass-Mitchell, T., Weber, R. J., Gentner, D. R., & Ng, N. L. (2023). Experiment set: Furans+OH_BrC_Joo [Dataset]. Integrated Chamber Atmospheric data Repository for Unified Science (ICARUS). https://icarus.ucdavis.edu/experimentset/262

Joo, T., Rivera-Rios, J. C., Takeuchi, M., Alvarado, M. J., & Ng, N. L. (2019). Secondary organic aerosol Formation from reaction of 3-methylfuran with nitrate radicals. *ACS Earth and Space Chemistry*, *3*(6), 922–934. https://doi.org/10.1021/acsearthspacechem.9b00068

Kampf, C. J., Filippi, A., Zuth, C., Hoffmann, T., & Opatz, T. (2016). Secondary brown carbon formation via the dicarbonyl imine pathway: Nitrogen heterocycle formation and synergistic effects. *Physical Chemistry Chemical Physics*, *18*(27), 18353–18364. https://doi.org/10.1039/C6CP03029G

Kebabian, P. L., Herndon, S. C., & Freedman, A. (2005). Detection of nitrogen dioxide by cavity attenuated phase shift spectroscopy. *Analytical Chemistry*, *77*(2), 724–728. https://doi.org/10.1021/ac048715y

Kirchstetter, T. W., Novakov, T., & Hobbs, P. V. (2004). Evidence that the spectral dependence of light absorption by aerosols is affected by organic carbon. *Journal of Geophysical Research: Atmospheres*, *109*(D21). Portico. https://doi.org/10.1029/2004jd004999

Koss, A. R., Sekimoto, K., Gilman, J. B., Selimovic, V., Coggon, M. M., Zarzana, K. J., et al. (2018). Non-methane organic gas emissions from biomass burning: Identification, quantification, and emission factors from PTR-ToF during the FIREX 2016 laboratory experiment. *Atmospheric Chemistry and Physics*, *18*(5), 3299–3319. https://doi.org/10.5194/acp-18-3299-2018

Lack, D. A., Bahreini, R., Langridge, J. M., Gilman, J. B., & Middlebrook, A. M. (2013). Brown carbon absorption linked to organic mass tracers in biomass burning particles. *Atmospheric Chemistry and Physics*, *13*(5), 2415–2422. https://doi.org/10.5194/acp-13-2415-2013

Laskin, A., Laskin, J., & Nizkorodov, S. A. (2015). Chemistry of atmospheric Brown carbon. *Chemical Reviews*, *115*(10), 4335–4382. https://doi.org/10.1021/cr5006167

Lee, A. K. Y., Zhao, R., Li, R., Liggio, J., Li, S.-M., & Abbatt, J. P. D. (2013). Formation of light absorbing organo-nitrogen species from evaporation of droplets containing glyoxal and ammonium sulfate. *Environmental Science and Technology*, *47*(22), 12819–12826. https://doi.org/10.1021/es402687w

Liu, J., Lin, P., Laskin, A., Laskin, J., Kathmann, S. M., Wise, M., et al. (2016). Optical properties and aging of light-absorbing secondary organic aerosol. *Atmospheric Chemistry and Physics*, *16*(19), 12815–12827. https://doi.org/10.5194/acp-16-12815-2016

Liu, P., Zhang, Y., & Martin, S. T. (2013). Complex refractive indices of thin films of secondary organic materials by spectroscopic ellipsometry from 220 to 1200 nm. *Environmental Science & Technology*, *47*(23), 13594–13601. https://doi.org/10.1021/es403411e

Liu, P. F., Abdelmalki, N., Hung, H. M., Wang, Y., Brune, W. H., & Martin, S. T. (2015). Ultraviolet and visible complex refractive indices of secondary organic material produced by photooxidation of the aromatic compounds toluene and *m*-xylene. *Atmospheric Chemistry and Physics*, *15*(3), 1435–1446. https://doi.org/10.5194/acp-15-1435-2015

Liu, S., Shilling, J. E., Song, C., Hiranuma, N., Zaveri, R. A., & Russell, L. M. (2012). Hydrolysis of organonitrate functional groups in aerosol particles. *Aerosol Science and Technology*, *46*(12), 1359–1369. https://doi.org/10.1080/02786826.2012.716175

Liu, S., Wang, Y., Wang, G., Zhang, S., Li, D., Du, L., et al. (2021). Enhancing effect of NO2 on the formation of light-absorbing secondary organic aerosols from toluene photooxidation. *Science of the Total Environment*, *794*, 148714. https://doi.org/10.1016/j.scitotenv.2021.148714

Lopez-Hilfiker, F. D., Mohr, C., Ehn, M., Rubach, F., Kleist, E., Wildt, J., et al. (2014). A novel method for online analysis of gas and particle composition: Description and evaluation of a filter inlet for gases and AEROsols (FIGAERO). *Atmospheric Measurement Techniques*, *7*(4), 983–1001. https://doi.org/10.5194/amt-7-983-2014

Mettler, M. S., Mushrif, S. H., Paulsen, A. D., Javadekar, A. D., Vlachos, D. G., & Dauenhauer, P. J. (2012). Revealing pyrolysis chemistry for biofuels production: Conversion of cellulose to furans and small oxygenates. *Energy and Environmental Science*, *5*(1), 5414–5424. https://doi.org/10.1039/C1EE02743C

Nguyen, T. B., Bates, K. H., Buenconsejo, R. S., Charan, S. M., Cavanna, E. E., Cocker, D. R., III, et al. (2023). Overview of ICARUS—A curated, open access, online repository for atmospheric simulation chamber data. *ACS Earth and Space Chemistry*, *7*(6), 1235–1246. https://doi.org/10.1021/acsearthspacechem.3c00043

Nozière, B., Dziedzic, P., & Córdova, A. (2009). Products and kinetics of the liquid-phase reaction of glyoxal catalyzed by ammonium ions (NH4+). *The Journal of Physical Chemistry A*, *113*(1), 231–237. https://doi.org/10.1021/jp8078293

Nozière, B., Dziedzic, P., & Córdova, A. (2010). Inorganic ammonium salts and carbonate salts are efficient catalysts for aldol condensation in atmospheric aerosols. *Physical Chemistry Chemical Physics*, *12*(15), 3864–3872. https://doi.org/10.1039/B924443C

Nozière, B., & Esteve, W. (2007). Light-absorbing aldol condensation products in acidic aerosols: Spectra, kinetics, and contribution to the absorption index. *Atmospheric Environment*, *41*(6), 1150–1163. https://doi.org/10.1016/j.atmosenv.2006.10.001

Palm, B. B., Peng, Q., Fredrickson, C. D., Lee, B. H., Garofalo, L. A., Pothier, M. A., et al. (2020). Quantification of organic aerosol and brown carbon evolution in fresh wildfire plumes. *Proceedings of the National Academy of Sciences of the United States of America*, *202012218*. https://www.pnas.org/content/pnas/early/2020/11/03/2012218117.full.pdf

Peng, Q., Palm, B. B., Melander, K. E., Lee, B. H., Hall, S. R., Ullmann, K., et al. (2020). HONO emissions from western U.S. Wildfires provide dominant radical source in fresh wildfire smoke. *Environmental Science and Technology*, *54*(10), 5954–5963. https://doi.org/10.1021/acs.est.0c00126

Pratt, K. A., Murphy, S. M., Subramanian, R., DeMott, P. J., Kok, G. L., Campos, T., et al. (2011). Flight-based chemical characterization of biomass burning aerosols within two prescribed burn smoke plumes. *Atmospheric Chemistry and Physics*, *11*(24), 12549–12565. https://doi.org/10.5194/acp-11-12549-2011

Price, D. J., Clark, C. H., Tang, X., Cocker, D. R., Purvis-Roberts, K. L., & Silva, P. J. (2014). Proposed chemical mechanisms leading to secondary organic aerosol in the reactions of aliphatic amines with hydroxyl and nitrate radicals. *Atmospheric Environment*, *96*, 135–144. https://doi.org/10.1016/j.atmosenv.2014.07.035

Reddington, C. L., Spracklen, D. V., Artaxo, P., Ridley, D. A., Rizzo, L. V., & Arana, A. (2016). Analysis of particulate emissions from tropical biomass burning using a global aerosol model and long-term surface observations. *Atmospheric Chemistry and Physics*, *16*(17), 11083–11106. https://doi.org/10.5194/acp-16-11083-2016

Schymanski, E. L., Ruttkies, C., Krauss, M., Brouard, C., Kind, T., Dührkop, K., et al. (2017). Critical assessment of small molecule identification 2016: Automated methods. *Journal of Cheminformatics*, *9*(1), 22. https://doi.org/10.1186/s13321-017-0207-1

Sheu, R., Fortenberry, C. F., Walker, M. J., Eftekhari, A., Stönner, C., Bakker, A., et al. (2021). Evaluating indoor air chemical diversity, indoor-to-outdoor emissions, and surface reservoirs using high-resolution mass spectrometry. *Environmental Science and Technology*, *55*(15), 10255–10267. https://doi.org/10.1021/acs.est.1c01337

Sheu, R., Hass-Mitchell, T., Ringsdorf, A., Berkemeier, T., Machesky, J., Edtbauer, A., et al. (2022). Emerging investigator series: Deposited particles and human lung lining fluid are dynamic, chemically-complex reservoirs leading to thirdhand smoke emissions and exposure. *Environmental Sciences: Atmosphere*, *2*(5), 943–963. https://doi.org/10.1039/D1EA00107H

Souri, A. H., Choi, Y., Jeon, W., Kochanski, A. K., Diao, L., Mandel, J., et al. (2017). Quantifying the impact of biomass burning emissions on major inorganic aerosols and their precursors in the U.S. *Journal of Geophysical Research: Atmospheres*, *122*(21), 12020–12041. https://doi.org/10.1002/2017JD026788

Stark, H., Yatavelli, R. L. N., Thompson, S. L., Kang, H., Krechmer, J. E., Kimmel, J. R., et al. (2017). Impact of thermal decomposition on thermal desorption instruments: Advantage of thermogram analysis for quantifying volatility distributions of organic species. *Environmental Science and Technology*, *51*(15), 8491–8500. https://doi.org/10.1021/acs.est.7b00160

Takeuchi, M., & Ng, N. L. (2019). Chemical composition and hydrolysis of organic nitrate aerosol formed from hydroxyl and nitrate radical oxidation of α-pinene and β-pinene. *Atmospheric Chemistry and Physics*, *19*(19), 12749–12766. https://doi.org/10.5194/acp-19-12749-2019

Tiitta, P., Leskinen, A., Hao, L., Yli-Pirilä, P., Kortelainen, M., Grigonyte, J., et al. (2016). Transformation of logwood combustion emissions in a smog chamber: Formation of secondary organic aerosol and changes in the primary organic aerosol upon daytime and nighttime aging. *Atmospheric Chemistry and Physics*, *16*(20), 13251–13269. https://doi.org/10.5194/acp-16-13251-2016

Tuet, W. Y., Chen, Y., Fok, S., Champion, J. A., & Ng, N. L. (2017). Inflammatory responses to secondary organic aerosols (SOA) generated from biogenic and anthropogenic precursors. *Atmospheric Chemistry and Physics*, *17*(18), 11423–11440. https://doi.org/10.5194/acp-17-11423-2017

Updyke, K. M., Nguyen, T. B., & Nizkorodov, S. A. (2012). Formation of brown carbon via reactions of ammonia with secondary organic aerosols from biogenic and anthropogenic precursors. *Atmospheric Environment*, *63*, 22–31. https://doi.org/10.1016/j.atmosenv.2012.09.012

Wong, J. P. S., Tsagkaraki, M., Tsiodra, I., Mihalopoulos, N., Violaki, K., Kanakidou, M., et al. (2019). Atmospheric evolution of molecular-weight-separated brown carbon from biomass burning. *Atmospheric Chemistry and Physics*, *19*(11), 7319–7334. https://doi.org/10.5194/acp-19-7319-2019

Xu, L., Crounse John, D., Vasquez Krystal, T., Allen, H., Wennberg Paul, O., Bourgeois, I., et al. (2022). Ozone chemistry in western U.S. wildfire plumes. *Science Advances*, *7*(50), eabl3648. https://doi.org/10.1126/sciadv.abl3648

Xu, W., Takeuchi, M., Chen, C., Qiu, Y., Xie, C., Xu, W., et al. (2021). Estimation of particulate organic nitrates from thermodenuder–aerosol mass spectrometer measurements in the North China Plain. *Atmospheric Measurement Techniques*, *14*(5), 3693–3705. https://doi.org/10.5194/amt-14-3693-2021

Zeng, L., Zhang, A., Wang, Y., Wagner, N. L., Katich, J. M., Schwarz, J. P., et al. (2020). Global measurements of Brown carbon and estimated direct radiative effects. *Geophysical Research Letters*, *47*(13), e2020GL088747. https://doi.org/10.1029/2020GL088747

Zhang, H., Surratt, J. D., Lin, Y. H., Bapat, J., & Kamens, R. M. (2011). Effect of relative humidity on SOA formation from isoprene/NO photooxidation: Enhancement of 2-methylglyceric acid and its corresponding oligoesters under dry conditions. *Atmospheric Chemistry and Physics*, *11*(13), 6411–6424. https://doi.org/10.5194/acp-11-6411-2011

Zhao, X., & Wang, L. (2017). Atmospheric oxidation mechanism of furfural initiated by hydroxyl radicals. *The Journal of Physical Chemistry A*, *121*(17), 3247–3253. https://doi.org/10.1021/acs.jpca.7b00506

References From the Supporting Information

Chen, Y., & Bond, T. C. (2010). Light absorption by organic carbon from wood combustion. *Atmospheric Chemistry and Physics*, *10*(4), 1773–1787. https://doi.org/10.5194/acp-10-1773-2010

Laskin, A., Laskin, J., & Nizkorodov, S. A. (2015). Chemistry of atmospheric brown carbon. *Chemical Reviews*, *115*(10), 4335–4382. https://doi.org/10.1021/cr5006167

Liu, J., Bergin, M., Guo, H., King, L., Kotra, N., Edgerton, E., & Weber, R. J. (2013). Size-resolved measurements of brown carbon in water and methanol extracts and estimates of their contribution to ambient fine-particle light absorption. *Atmospheric Chemistry and Physics*, *13*(24), 12389–12404. https://doi.org/10.5194/acp-13-12389-2013